JOURNAL OF MATERIALS SCIENCE 25 (1990) 1491–1496

Effect of carbon on the weldability of Fe–Mn–Al alloys

CHANG-PIN CHOU, CHIEN-HSUN LEE
Department of Mechanical Engineering, National Chiao-Tung University, Hsinchu, Taiwan

Based on the composition of 30% Mn, 10% Al, balance Fe, Fe–Mn–Al alloys with different carbon contents and thus different ferrite contents were studied. Tensile tests and U-bend tests on the autogenous GTA welded specimen were utilized to evaluate the weldability. FN measurement, optical metallography, and SEM-EDAX were used to study the microstructural characteristics of the weld metal and the base metal heat affected zone. It was found that the carbon content has a strong influence on the amount of residual ferrite in the Fe–Mn–Al weld metals studied. After heat treatment, the amount of residual ferrite is reduced and annealing twins were found in the weld metal. Tensile strengths in excess of 900 MPa in both the longitudinal and transverse welding directions were obtained. The elongation of the butt-joint-welded specimen is substantially less than that of the base metal, especially for the fully austenitic weld metal. U-bend test results gave an indication of good weldability for the Fe–Mn–Al alloys.

1. Introduction

Recently, Fe–Mn–Al alloys have been considered promising replacements for austenitic stainles steels. Aluminium and manganese are used to replace the expensive alloying elements in the conventional Fe–Cr–Ni system. This alloy system also has long-range strategic advantages [1].

Aluminium plays a major role in the oxidation and corrosion resistance which is characteristic of the binary Fe–Al alloy. Manganese is an austenite stabilizer which together with carbon has the capability of retaining the face-centred-cubic austenitic structure [2]. Hence, a suitable composition of iron, manganese, aluminium and carbon should give an austenitic alloy with good mechanical properties and oxidation resistance.

The Fe–Mn–Al alloys were first developed in the 1930s. Korter and Tonn [3] established a partial phase diagram in which three phase regions containing ferrite, austenite and duplex (ferrite and austenite) were mapped out, respectively. Later, this was generally confirmed and slightly modified. In 1958, Ham and Carins [4] proposed the composition Fe–34.4Mn–10.2Al–0.76C, on development of a promising candidate in the Fe–Al–Mn alloy family. They called it a poor man's stainless steel because it possessed high potentials of low price and promising corrosion resistance. After ageing between 550 and 750° C, carbon-containing Fe–Mn–Al alloy could be further strengthened by precipitating the K phase [5, 6]. In general, silicon or chromium addition was beneficial to high-temperature oxidation and corrosion resistance [7–9]. Furthermore, with the addition of silicon, the marine corrosion resistance and cavitation erosion resistance could be enhanced. Therefore, Si-added Fe–Mn–Al alloy was used for the propellers of seagoing vessels launched in 1980 [10].

Based on the composition of Fe–30Mn–10Al–1.0C alloy, Wan and co-workers [11–15] found that Fe–Mn–Al stainless steels are good candidates for replacing at least part of the conventional Fe–Cr–Ni stainless steels; and that these alloys possessed significant cost and density advantages, good mechanical properties, excellent corrosion and oxidation resistance. If these alloys are to be used in practical situations, the weldability must be assessed. The weldability of a series of Fe–Mn–Al alloys has been studied in our previous study [16–20]. As part of the sequential programme, some preliminary results are reported in this paper.

2. Experimental procedure

Three compositions of Fe–Mn–Al–C were prepared from pure iron (99%), electrolytic manganese (99.96%), high-purity aluminium (99.99%), and high-purity carbon. The alloys were prepared in a vacuum induction furnace of pressure under 10^{-2} torr and cast under an argon atmosphere. The as-cast alloys were subsequently hot forged to 8 mm thick at 1200° C, then homogenized at 1050° C for 12 h. Some of the homogenized billets were cold rolled to 4 mm thick plates and annealed at 950° C for 1 h in an argon atmosphere furnace, followed by water quenching.

TABLE I Chemical compositions (wt %) of the investigated alloys

Alloy	Fe	Mn	Al	C	S
A	bal.	28.44	7.96	0.53	0.006
B	bal.	29.28	8.59	0.81	0.004
C	bal.	29.05	8.03	1.17	0.001

0022–2461/90 $03.00 + .12

TABLE II Welding parameters used in autogenous GTA welding in this study

Welding condition	Voltage (V)	Current (A)	Travel speed (mm min^{-1})	Flow rate (m^3 h^{-1})	Electrode (mm)	Heat input (kJ mm^{-1})
1	8.5	80	150	1.27	1.59	0.27
2	9.8	105	150	1.42	1.59	0.41
3	10.5	140	150	1.42	1.59	0.59
4	13.8	220	150	1.42	2.38	1.21
5	14.0	260	150	1.42	2.38	1.46

The compositions of these alloys were analysed by inductively coupled plasma–atomic emission spectrometry (ICP–AES) and the results are listed in Table I.

Autogenous gas tungsten arc (GTA) welds were made using the direct current electrode negative (DCEN) condition. Several welding conditions were applied in this investigation; they are listed in Table II. The dimensions and weld bead configuration of the as-welded plate are shown in Figs 1a to c, the U-bend tests and tensile tests were conducted after welding. The welding condition applied in these thinner plates is condition 1 in Table II. In Fig. 1d, two parallel, overlapped remelt passes, which were welded under welding conditions 2, 3, 4 and 5, respectively, were made so that hot-crack susceptibility of weld metal, weld metal heat affected zone (HAZ), and base metal heat affected zone could be tested under the U-bend test.

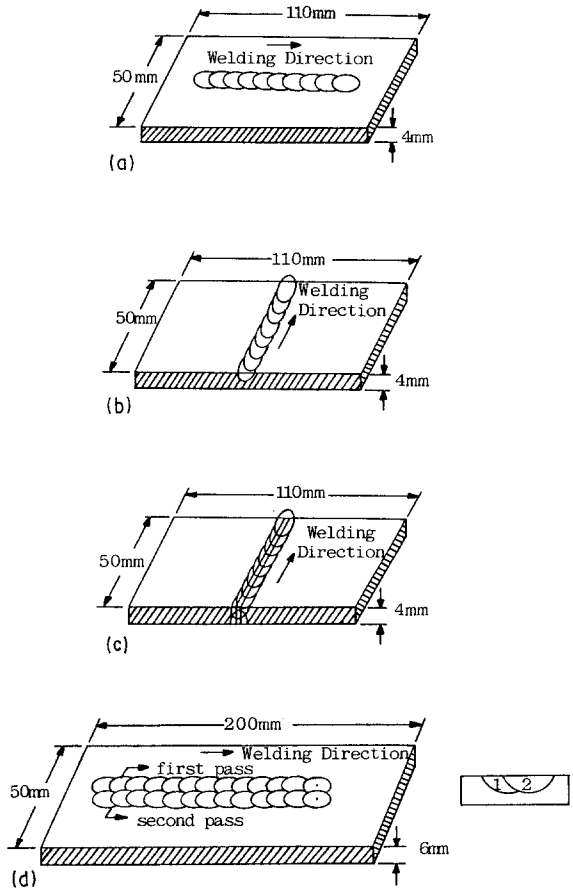

Figure 1 Dimensions and weld bead configuration of specimens for the U-bend and/or tensile tests. (a) Autogeneously welded (condition 1), longitudinal specimen. (b) Autogenously welded (condition 1), transverse specimen. (c) Butt-joint-welded (condition 1), transverse specimen. (d) Overlapped remelting (conditions 2, 3, 4 and 5), longitudinal specimen (U-bend test only).

The weld metal was heat treated at 1050° C for various times ranging from 5 to 240 min in an atmosphere-controlled furnace and then water quenched to room temperature.

The ferrite number (FN) of the base metals, weld metals and various heat-treated weld metals was measured using the Magne Gauge and the results are listed in Table III.

Standard tensile and U-bend tests were utilized to determine the effect of composition and welding conditions on the weldability of the Fe–Mn–Al–C alloys. Metallographic samples were prepared and etched with 10% nital. SEM with EDAX was also applied to detemine the chemical composition in selected regions of the structure.

3. Results and discussion

The ferrite number results in Table III show that it is influenced by the carbon content and welding conditions. Because carbon is a strong austenite former, the residual ferrite number of the base metal decreased from 3.5 to 0 as the carbon content increased from 0.6 to 1.1 wt %. Figure 2 shows the micrographs of base metal of alloys A and C. As can be seen, a small amount of globular-like ferrite can be observed in alloy A, while alloy C is fully austenitic structure in nature. After welding, the ferrite content is higher in the weld metal than in the base metal. Furthermore, the higher the welding heat input is, the higher is the ferrite number as shown in Table III. The possible causes that result in increase in ferrite number after welding might be the phase transformation during the solidification process and/or dissipation of the composition element, e.g. manganese or carbon, during the welding process.

Figure 3 is an optical micrograph of the weld metal investigated in this study. In the central portion of the weld pool, a typical equiaxed dendritic structure was found, especially in higher heat input conditions, e.g. condition 5 in Table II, as shown in Fig. 3a. Away from the central portion of the weld pool, the columnar structure could be observed as shown in Fig. 3b. In

TABLE III Ferrite number (FN) of base metals and weld metals welded under welding conditions 1 to 5

Alloy	FN					
	Base metal	Weld metals				
		1	2	3	4	5
A	3.5	10.4	12.3	12.8	13.5	13.8
B	0.0	3.5	4.7	5.0	5.4	5.6
C	0.0	0.3	0.4	0.4	0.5	0.9

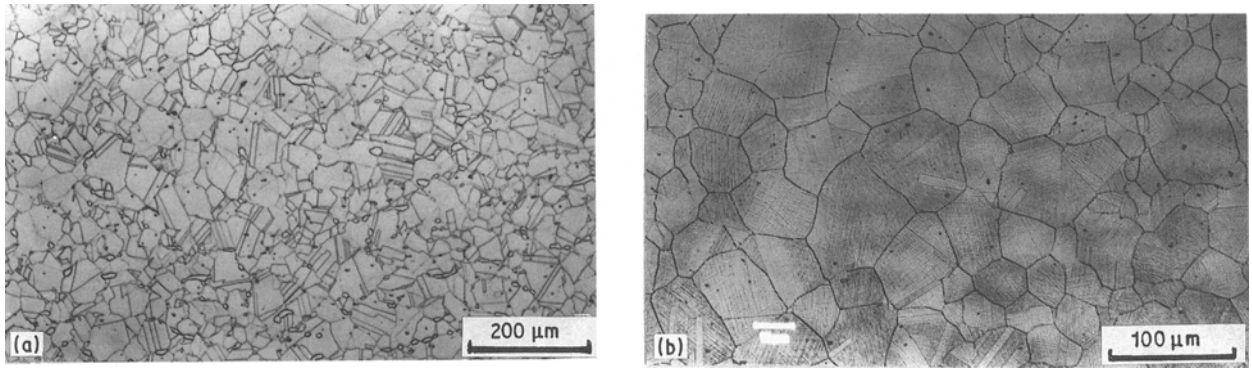

Figure 2 Microstructures of Fe–Mn–Al–C base metals (a) A and (b) C.

1956, Tiller and Rutter [21] proposed a relationshp between the solidification mode and the temperature gradient (G) and the growth rate (R) of the weld metal. Low values of $G/R^{1/2}$ indicated an increased tendency for constitutional supercooling, thus favouring the equiaxed dendritic or columnar dendritic mode of solidification, whereas high values of $G/R^{1/2}$ favoured the cellular mode. In 1965, Savage *et al.* [22] reported that equiaxed dendritic growth was observed in the central part of the crater, due to sufficient supercooling (or low $G/R^{1/2}$). In the central portion of the weld pool, the growth rate is greater and the temperature gradient is low enough, especially at high heat input, to form equiaxed dendritic structure, as shown in Fig. 3a. In the outer part of the weld pool, the temperature gradient is increased and the growth rate is decreased, therefore, the columnar dendritic mode is favoured, as shown in Fig. 3b. Evidence of epitaxial growth was found where the weld pool grew directly from the fusion line as shown in Fig. 3c.

After heat treating at 1050° C, the residual ferrite transformed into austenite. Fig. 4 shows a micrograph of weld metal A which has been heat treated for various times at 1050° C. It is seen that the ferrite content of heat-treated weld metal A is decreased to that of the base metal when the annealing time is longer than 120 min. The cause of the decrease in ferrite is probably due to the homogenization of compositional microsegregation. Savage *et al.* [22], indicated that microsegregation is unavoidable in the solidification process produced by welding. Microsegregation means that the solute concentration in the solidified metal differs with solidification temperature during the solidification process of welding. In this study, the solute concentrations, e.g. carbon, aluminium and manganese, within the liquid and solidified metal changed as the temperature of the weld decreased from the liquidus to the solidus temperature, even to the lower temperature region. This caused the solute concentration in the primary solidified region to be different from that of the last region solidified. In the region of lower carbon content, the structure is ferritic (b c c) type, whereas the structure is austenitic (f c c) type in the regions with higher carbon content. This might indicate that the increase of ferrite number after welding is partially due to microsegregation of the solute. After annealing at 1050° C, the microsegregation of the solute would be eliminated through the diffusion process and thus lower the ferrite content. The final ferrite content would reach a steady value which is the equilibrium

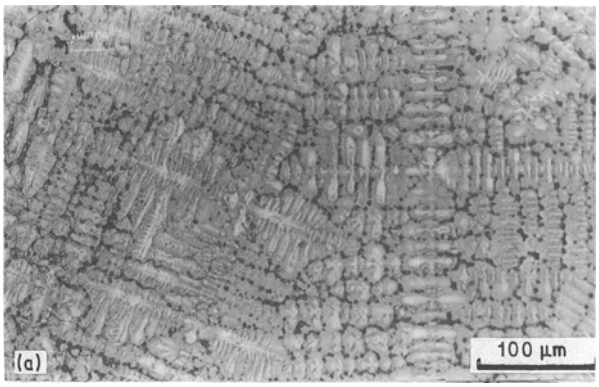

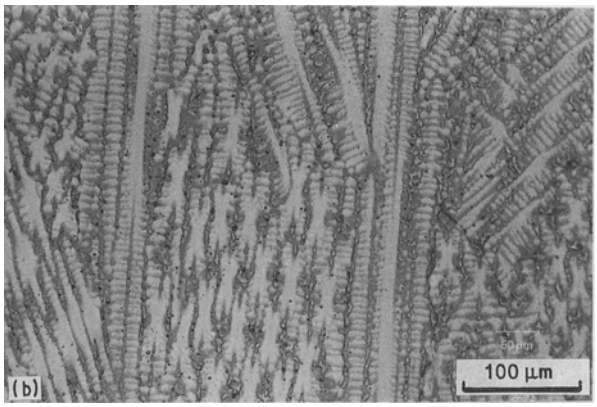

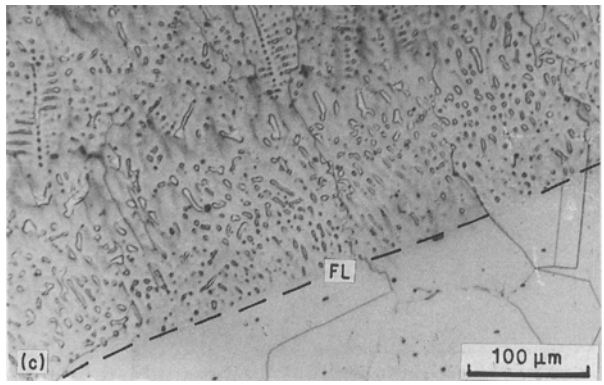

Figure 3 Microstructures of Fe–Mn–Al–C weld metals welded under condition 5. (a) Equiaxed dendritic structure of weld metal A. (b) Columnar dendritic structure of weld metal C. (c) Expitaxial growth taken near fusion line of weld metal B.

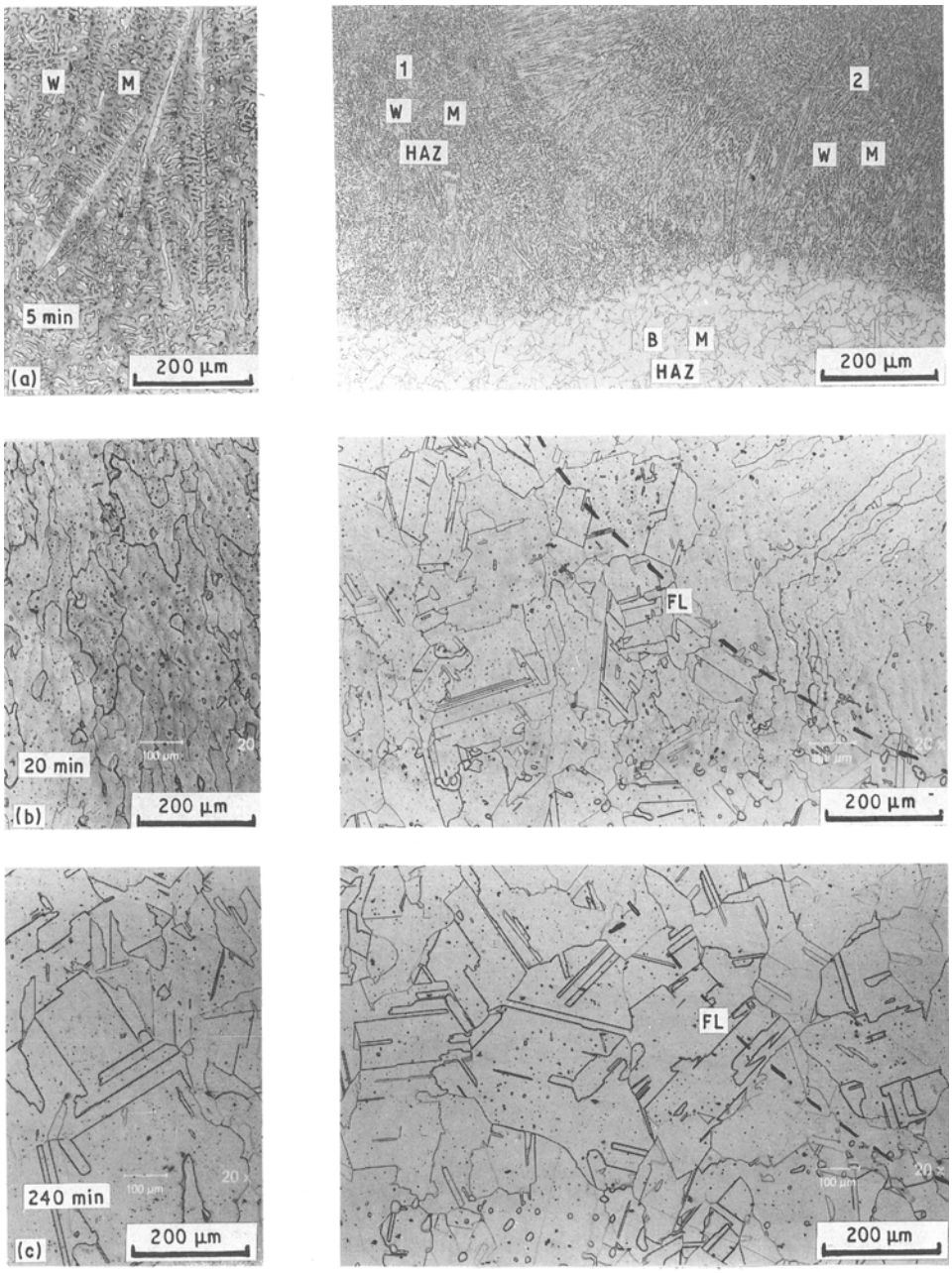

Figure 4 Optical micrograph of weld metal A with different annealing times. (a) 1050° C, 5 min; (b) 1050° C, 20 min; (c) 1050° C, 240 min.

value corresponding to the alloy's composition and annealing temperature.

Figure 4 shows another interesting phenomenon. After heat treatment for 20 min, annealing twins were observed in the weld metal HAZ. The weld metal HAZ in the first weld pass is adjacent to the second weld pass. When the annealing time is longer than 120 min, the annealing twins extended throughout the weld metal, and, the weld and base metals could not be distinguished by microscopic observation. According to Dieter [23], the presence of annealing twins in the microstructure is a good indication that the metal has been subjected to mechanical deformation prior to annealing, because it is likely that they grow from twin nuclei produced during transformation. Hertzberg suggested that annealing twins were generated in alloys with preexisting plastic deformation, then formed in associated with the growth of recrystallized grains from previously deformed material possessing a high density of stacking faults [24]. In this study, the deformation or distortion would occur due to the local heating during welding [25]. Therefore, annealing twins would be observed in the weld metal after heat treating at elevated temperature, But in the region of weld metal HAZ, the weld metal had been heat treated at least one thermal cycle from subsequent passes before the artificial solution treatment. Thus, the nuclei of annealing twins would grow earlier in weld metal HAZ than in other regions of weld metal which were not affected by the subsequent weld pass.

Tensile tests were conducted on the autogenously welded specimens in both the longitudinal and transverse directions. In order to determine the joint strength, the butt-joint-welded specimens were also tested in the transverse direction. The results are presented graphically in Fig. 5. Typical results from conventional Fe–Cr–Ni austenitic stainless steels are also presented for comparison. All three Fe–Mn–Al alloys show promising strength and ductility in the autogenously welded conditions. Alloy C is the

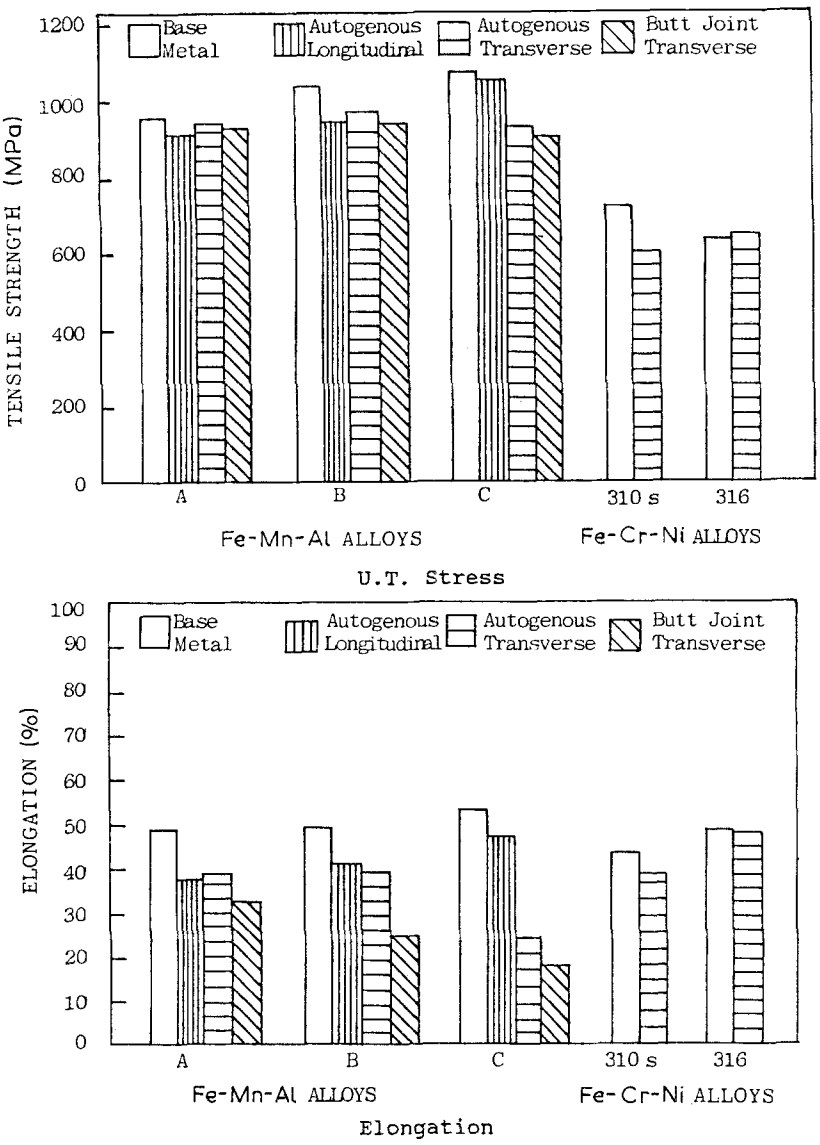

Figure 5 Tensile test results of Fe–Mn–Al–C weld metals A, B and C.

strongest, but in the butt-joint-welded condition, alloy C shows an inferior result. The elongation is reduced from 54% in the unwelded condition to only 19%. The tensile specimens fractured at the centre line of the weld metal. This is probably due to the enhanced segregation of alloying solute and impurity elements in the central part of a weld bead. An SEM fractograph of weld metal A is shown in Fig. 6; this reveals a typical ductile fracture surface with uniform dimples. The fracture dimples appeared to have been initiated by aluminium-rich particles (confirmed by SEM–EDAX analysis).

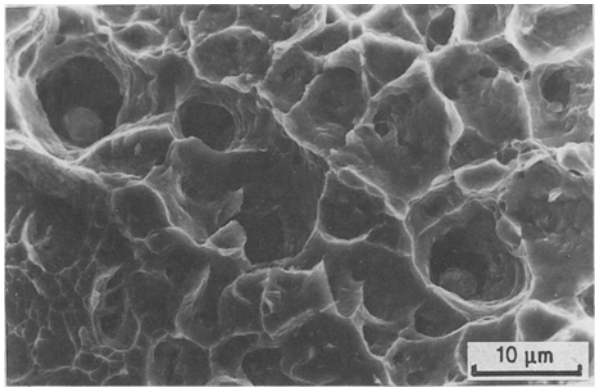

Figure 6 SEM micrograph of fractured surface of tensile tested weld metal A.

Promising results were obtained for the butt-joint-welded specimens when U-bend tested in the transverse direction. No cracking was observed for any of the welding conditions tested.

4. Conclusions

1. The carbon content in Fe–Mn–Al alloys has a strong influence on the residual ferrite content of the metal is reduced as the carbon content in the alloy is increased.

2. The preliminary results of weldability testing show that the Fe–Mn–Al–C weld metal has excellent strength (> 900 MPa) and ductility (> 20%).

Acknowledgements

This research was sponsored by the National Science Council of the Republic of China under grant NSC 74-0405-E009-002. The authors also thank Professor C. M. Wan for encouragement and helpful discussions during the course of this work.

References

1. J. CHARLES, A. BERGHEZAN, A. LUTTS and P. DANCOISNE, *Metal Progr.* **116** (1981) 71.
2. S. BANERJI, *ibid.* **31** (1978) 59.

3. W. KORTER and W. TONN, *Archiv Eisenhuttenw.* **7** (1933) 365.
4. J. L. HAM and R. E. CARINS, *Product Engng* **52** (1958) 59.
5. G. S. KRIVONOGOV, M. F. ALEKSEYENKO and G. G. SOLOVYEVA, *Phys. Met. Metallogr.* **4** (1975) 86 (English Translation).
6. N. A. STORCHAK and A. G. DRACHINSKAYA, *ibid.* **44** (1977) 123.
7. H. ERHART, R. WANG and R. A. RAPP, *Oxid. Metals* **21** (1984) 81.
8. R. WANG, M. J. STRASZHEIM and R. A. RAPP, *ibid.* **21** (1/2) (1984) 35.
9. P. R. S. JACKSON and G. R. WALLWORK, *Oxid. Metals* **21** (3/4) (1984) 135.
10. R. WANG and F. H. BECK, *Metal Progr.* **36** (1983) 72.
11. C. L. TARN, C. T. HU and C. M. WAN, *Chinese J. Mater. Sci.* **15A** (1983) 75.
12. T. F. LIU, C. M. WAN and B. K. LEE, *ibid.* **15A** (1983) 11.
13. J. G. DUH, S. H. HUARNG and C. M. WAN, *ibid.* **16A** (1984) 14.
14. T. F. LIU and C. M. WAN, *Scripta Metall.* **19** (1985) 727.
15. T. S. SHEU, S. C. CHANG and C. M. WAN, *Chinese J. Mater. Sci.* **17A** (1985) 27.
16. C. P. CHOU and C. H. LEE, *Scripta Metall.* **23** (1989) 901.
17. *Idem., Metallography* in press.
18. *Idem., Metall. Trans.* in press.
19. *Idem., Scripta Metall.* **23** (1989) 1109.
20. *Idem., Mater. Sci. Engng.* in press.
21. W. A. TILLER and J. W. RUTTER, *Canad. J. Phys.* **34** (1956) 96.
22. W. F. SAVAGE, C. D. LUNDIN and A. H. OLSON, *Welding J.* **44** (1965) 1s.
23. G. E. DIETER, in "Mechanical Metallurgy" (McGraw-Hill, New York, 1976) p. 138.
24. R. W. HERTZBERG, in "Deformation and Fracture Mechanics of Engineering Materials" (Wiley, New York, 1983) p. 106.
25. K. MASUBUCHI, in "Analysis of Welded Structures-Residual Stress, Distortion and Their Consequences", (Pergamon, New York, 1980) p. 2.

Received 24 October 1988
and accepted 1 June 1989